Mathematical modeling of flows in porous media.

Dushin V.R.*, Nikitin V.F.*, Legros J.C., Silnikov M.V.*****

* Moscow M.V. Lomonosov State University, Moscow 119992,
RUSSIA
**Free University of Brussels, Brussels 1050,
BELGIUM
*** Saint Petersburg State Polytechnical University, 29 Politechnicheskaya Str.,
195251 St. Petersburg
RUSSIA
vrdush@rambler.ru

Abstract - The paper is aimed at mathematical modeling of flows in porous medium. The results are compared with model experiments performed under microgravity conditions. Numerical investigations of the instability in displacement of viscous fluid by a less viscous one in a two-dimensional and three-dimensional geometry were carried out. The effect of the three-dimensional phenomena on instability growth was investigated.

Key-Words: - porous medium, seepage, flow, capillary, unstable, microgravity

1. Introduction

The background for the performed research is the following. Dimensions analysis of the governing system of equations shows that surface tension relevant effects turn to be essential in the momentum equations for small Bond numbers: $C_m = \frac{(\rho_1 - \rho_2) g r_*^2}{\sigma_{12}}$. Thus, to measure the capillary forces accurately one needs to reduce the Bond number C_m as much as possible. It could be done by various means: decreasing the density difference $(\rho_1 - \rho_2)$, increasing the surface tension (σ_{12}), decreasing the pore size(*r)* and decreasing the gravity acceleration (*g)*. The first three groups of parameters are those characterising the media under investigation. Thus, these parameters could not be varied arbitrary. The last of the parameters – $\vec{g}$ – characterises the environment for the experiment. It could be varied without affecting the media properties.

Microgravity environment provides a unique possibility to reduce the C_m parameter practically as low as necessary to get the needed accuracy of measurements. Besides, using the microgravity environment one can essentially increase the characteristic pore size r_* to study the microscopical capillary processes, maintaining the small value of the capillary microgravity parameter C_m.

The problem is relevant to a hydrocarbon recovery, which is performed by the flow of gas under a pressure differential displacing the high viscosity fluid. Entrapment of high viscosity fluid by the low viscosity fluid flow lowers down the quality of a hydrocarbon recovery leaving the most of viscous fluid entrapped thus decreasing the production rate. The developed models and obtained results are applicable to description of liquid non-aqueous phase contaminants underground migration, their entrapment in the zones of inhomogenity, and forecasting the results of remediatory activities in the vicinities of waste storages and contaminated sites.

Experimental investigations were performed using artificial porous medium. The artificial

porous medium was composed of glass spheres. This type of a medium preserves all the characteristic features of the natural porous medium and allows direct optical registration of flow peculiarities.

The motivation to develop the present theoretical approach to capillary driven filtration modelling was the following. The widely used generalised Darcy law and capillary seepage equations[1-3] are based on the assumption of local equilibrium phase distribution in an elementary volume of a porous medium. In particular, it is assumed that: (1) the effect of viscous drag and inertia on phase distribution in pores is negligibly small being compared with capillary forces action; (2) each phase is moving in its own system of pore channels and interaction between fluid phases could be neglected in comparison with the interaction between fluids and the skeleton; (3) all the changes of saturation take place in a quasi-static equilibrium way and are independent on the flow regime. But usually in the flows of two immiscible fluids in a porous medium, the non-equilibrium phenomena caused by the delay of establishing the equilibrium phase distribution after a saturation change, are of no less importance than the direct influence of viscous forces [1]. Establishing equilibrium phase distribution demands a certain time interval, which depends on the processes taking place in a "macroscopically small" volume (an ultimate degree of space discretization permitted in the seepage theory). Thus the characteristic time τ_{cap}^{eq} is introduced depending on the discretization scale, which separates the slow processes of two-phase flow, to which the quasi-equilibrium theory is applicable, from the "fast processes", which could be considerably influenced by non-equilibrium effects. Such non-equilibrium processes occur in hydraulic fracturing [4], wherein the characteristic time of fracture propagation is much less than τ_{cap}^{eq} [5].

Capillary seepage processes in granular beds under microgravity conditions were investigated in [6-8]. The model introduced empirical coefficients to be measured experimentally. To provide non-equilibrium conditions experiments on capillary driven imbibition under microgravity were performed [8].

The present paper gives the coverage of some results on capillary driven seepage flows porous media incorporating multidimensional inhomogeneties. The role of permeability non-uniformity in determining the mean seepage rate in drainage and imbibition is investigated.

2. Mathematical model

The theoretical model accounting for the influence of capillary forces in multiphase filtration of immiscible fluids in porous media, developed in [7-10] introduced rheological relationships to determine the capillary forces. The full set of equations for the general case can be found in [7,9]. Here we shall use the developed model for investigating capillary driven filtration in porous media of variable properties. We shall assume that there is no mass transfer between phases. Then the mass and momentum equations for phases have the form:

$$\frac{\partial \alpha_i \rho_i}{\partial t} + div(\alpha_i \rho_i \vec{u}_i) = 0 \quad i = 1,\ldots,N \quad (1)$$

$$\frac{\partial \alpha_i \rho_i \vec{u}_i}{\partial t} + \mathrm{div}(\alpha_i \rho_i \vec{u}_i \vec{u}_i) = -\alpha_i \mathrm{grad}(p_i) + \alpha_i \mathrm{grad}(p_{ci}) - \alpha_i \rho_i \vec{g} + \mathrm{div}(\vec{J}_i) - \sum_{j=1}^{N} \vec{F}_{ij} \quad ; \quad (2)$$

and the rheological relationships for the introduced notation of averaged capillary pressures:

$$p_{c_k} = \frac{1}{\alpha} \sum_{j=1}^{N} \alpha_j p_{c_{kj}}(\sigma_{kj}, r_*, \theta_{kj}, \chi_{kj}^1, \chi_{kj}^2, \ldots), \quad (3)$$

where $\rho_i, \vec{u}_i, \alpha_i, p_i$ – density, velocity, volume fraction, pressure of the i-th phase; $\vec{g}$ – mass forces density; $\vec{J}_i$ – viscous stress tensor; $\vec{F}_{ij}$ – forces of phase interactions, incorporating microscopical viscous and inertial forces; $p_{c_{kj}} = \frac{1}{S_{kj}} \iint_{S_{kj}} \sigma_{kj} K_S ds$ is a capillary tension on the interface separating k-th and j-th phases

and positive direction of the normal vector to the interface is assumed to be from k-th to j-th phase thus the sign of mean curvature $\boldsymbol{K_S}$ of the interface S_{kj} determining the sign of capillary tension (or pressure).

The positive direction for the introduced capillary tension $p_{c_{kj}}$ coincides with the external normal vector to an elementary interface separating the k-th phase while positive pressure gives the tension of the opposite orientation $\vec{p}_{nk} = -p_k \vec{n}$. Thus due to our definitions we have opposite signs in front of gradients in the equation (2).

The rheological investigations [7] showed that capillary pressure can be the following function:

$$p_{c_{kj}} = f(\sigma_{kj}, r_*, \theta_{kj}, \chi_k^1, ... \chi_k^n),$$

where σ_{kj} – surface tension at the interface, separating the k-th and j-th phases; θ_{kj} – wetting angle; r_* – characteristic pore size; $\chi_k^1 ... \chi_k^n$ – dimensionless parameters characterising preimbibition of the solid matrix, saturation, shape of the interfaces, etc.; $\theta_{kj} = \varphi_{kj}(\rho_k, \rho_j, \mu_k, \mu_j, \sigma_{kj}, r_*, \vec{u}_{kj}, \chi_{kj})$ – the dynamic contact angle can depend on velocity of the contact line viscous and inertial properties of fluids, etc.

The following dimensionless combinations can be arranged from the parameters involved:

$$\mathrm{Ca}_k = \frac{\mu_k u_{kj}}{\sigma_{kj}}; \qquad \mathrm{Ca}_j = \frac{\mu_j u_{kj}}{\sigma_{kj}};$$

$$\mathrm{We}_k = \frac{\rho_k u_{kj}^2 r_*}{\sigma_{kj}}; \quad \mathrm{We}_j = \frac{\rho_j u_{kj}^2 r_*}{\sigma_{kj}}. \quad (4)$$

Then the formula (3) can be transformed into the relationship of dimensionless parameters:

$$\frac{p_{c_{kj}} \cdot r_*}{\sigma_{kj}} = \Psi_{kj}(Ca_k, Ca_j, We_k, We_j, \chi_k^1, ... \chi_k^n) \quad (5)$$

Thus, the universal dimensionless functional parameter Ψ_{kj} can be introduced as a main characteristic determining the capillary forces in porous media. Introducing one mean value r_* as a characteristic pore size is of course a serious simplification as in a real porous medium a network of pores is usually connected by smaller capillaries distributed in a random manner. The capillary pressure in smaller capillaries is much larger then the average capillary pressure that brings in drainage to appearing of irreducible saturation of the wetting phase. That should cause different behaviour of a wetting fluid capillary creeping into dry or preimbibitted unsaturated porous media. These effects were detected in microgravity experiments on capillary driven filtration and discussed in [7]. But introducing mean value for the characteristic pore size is nevertheless acceptable and rather convenient because, the influence of preimbibition can be taken into account defining the dimensionless Ψ-factor. The characteristic radius will be determined as the one for a cylindrical capillary providing drag forces similar to that in a porous medium under the same flow rate: $r_* = 2\sqrt{2K}$.

The successive derivations will be aimed at deriving from the basic conservation equations (2) the Darcy formulae for multiphase fluid filtration in porous matrix. Usually the Darcy equations for multiphase fluid filtration are obtained in a different manner — by generalising the Darcy formula derived for one fluid [1-3]. Our derivations will make it possible to obtain a more accurate form of the Darcy equations for multiphase flows and to find out actual approximations bounding the validity of the existing equations of the equilibrium seepage theory.

The mean forces accounting for phase interactions can be determined by the following formulae [2,3]:

$$\vec{F}_{ij} = \begin{cases} \frac{1}{2} C_{fij} \rho_i (\vec{u}_i - \vec{u}_{ij}) \,|\, \vec{u}_i - \vec{u}_{ij} \,|\, S_{ij}; & i \neq j \\ \frac{1}{2} C_{fij} \rho_i \ (\vec{u}_i - \vec{u}_s) \,|\, \vec{u}_i - \vec{u}_s \,|\, S_{ii}; & i = j \end{cases}$$

where F_{ii} is the force due to the interaction of the *i*-th phase with the porous matrix, $\vec{u}_{ij}$ is the velocity of the interface between the *i*-th and *j*-th phases, $\vec{u}_s$ is the velocity of the solid matrix (in most cases it is assumed to be zero,

$\vec{u}_s = 0$), S_{ij} is the area of contact between the *i*-th and *j*-th phases per volume unit, S_{ii} is the area of contact between the *i*-th phase and the solid porous matrix. The drag coefficient usually depends on the Reynolds number in the following way :

$$C_{fij} = C_f^0\left(\frac{1}{\mathrm{Re}_{ij}} + k_2\right), \qquad \mathrm{Re}_{ij} = \rho_i\left|\vec{u}_i - \vec{u}_{ij}\right| \cdot 2r_* / \mu_i \quad . \quad (7)$$

The velocity at phase interfaces could be determined based on the conditions of matching

$\vec{F}_{ij} = -\vec{F}_{ji}; \quad S_{ij} = S_{ji}; \quad \vec{u}_{ij} = \vec{u}_{ji};$

that gives the following formula :

$$\vec{u}_{ij} = \vec{u}_i + \frac{\mu_j}{\mu_i + \mu_j}(\vec{u}_j - \vec{u}_i) \quad (8)$$

On introducing the following notation for saturation of the matrix with the *i*-th phase $s_i = \alpha_i / \alpha$ one could assume the formula for the area of interfaces: $S_{ij} = S \cdot \frac{4}{3} s_i \cdot s_j, i \neq j; S_{ii} \cdot S\ s_i$, where S is the mean area of pores per volume unit ($S = \alpha / 2r_*$). Substituting the above notations in momentum equation for the *i*-th phase (2), neglecting inertial terms as it is done in the seepage theory for low filtration velocities, and assuming interface drag being collinear to the *i*-th velocity vector, one obtains the generalisation of Darcy equation for multiphase flow:

$$\vec{u}_i = -\frac{KK_{ir}}{\mu_i} \cdot (\mathrm{grad}\, p_i - \mathrm{grad}\, p_{ci} + \rho_i \vec{g}), \quad (9)$$

where permeability coefficient for the matrix accounting for (10) is determined as follows :

$$\frac{1}{K} = \frac{1}{2} C_f^0 \frac{S}{\alpha \cdot\cdot 2r_*} = \frac{1}{2} \frac{C_f^0}{(4r_*)^2}$$

Coefficient K_{ir} could be named a relative permeability coefficient for the *i*-th phase. The undertaken derivations showed that even within the frames of all the above assumptions relative permeability coefficient should be a function of relative velocities of phases and their volume fraction:

$$K_{ir} = \left(1 + \sum_{i \neq j} \frac{\mu_j}{\mu_i + \mu_j} \cdot \frac{\beta_j |\vec{u}_j - \vec{u}_i|}{|\vec{u}_i|} s_j\right)^{-1}$$

Very often mean flux velocities are introduced in the seepage theory as follows: $\vec{v}_i = \alpha_i \vec{u}_i$, that brings to a different form of permeability coefficients to keep the form of the equation (10) :

$$k = \alpha K; \quad f_i = s_i K_{ir}.$$

Introducing the relative permeability as a function of saturation only, as it is always done in the seepage theory, thus is not consistent, as one can see it being dependent on velocities. (8)

The derived formula (12) defining relative permeability is, nevertheless, an approximate one based on a number of assumptions (9) concerning internal flow and geometry of pores. Thus relative permeabilities are more often determined experimentally though the necessary precision could not be guaranteed for multiphase filtration. To avoid the necessity of taking into account the interaction at fluid-fluid phase interfaces one should derive the equations for the mean flow of the mixture.

To derive the equations for the mean flow we introduce the following notations:

$\rho = \frac{1}{\alpha}\sum_i \alpha_i \rho_i$ – density of the mixture;

$\alpha = \sum_i \alpha_i$ – porosity of the mixture;

$\vec{u} = \sum_i \frac{\alpha_i \rho_i \vec{u}_i}{\alpha \rho}$ – mean mass velocity; (10)

$\vec{w}_i = \vec{u}_i - \vec{u}$ – diffusive velocity; $\vec{I}_i = \frac{\alpha_i \rho_i \vec{W}_i}{\alpha}$ – diffusive flux.

For the case of two fluids capillary affected filtration, under the conditions $\rho_2 << \rho_1$ (the fluid 2 is gas) the formula (5) defining the local capillary pressure takes the form:

$$p_{c_{12}} = \frac{\sigma_{12}}{r_*} \psi_{12}(Ca_1, s, \chi_i), \quad (13)$$

where the dimensionless ψ_{12}-factor could be the function of capillary number, saturation, and other parameters characterizing shapes of interfaces, roughness of the surfaces, the flow history, etc. Then using the definition for the bulk capillary pressure (3) one obtains:

$$p_{c1} = \frac{1}{\alpha}\sum_{i=1}^{2}\alpha_i p_{c12} = (1-s)\frac{\sigma_{12}}{r_*}\psi_{12}. \quad (14)$$

For the case of two fluids filtration, we will use the following definitions :

$$s_1 = s;\ s_2 = 1-s;\ \vec{I}_1 = -\vec{I}_2 = \vec{I} = \alpha s(\vec{u}_1 - \vec{v});$$

$$\mu = \mu_1 s + \mu_2(1-s).$$

Then, assuming the porous matrix non-deformable the system of equation (1,2) takes the following form:

$$\frac{\partial s\alpha}{\partial t} + \mathrm{div}(s\alpha\vec{v}) = -\mathrm{div}(\alpha\vec{I}), \quad (15)$$

$$\mathrm{div}(\alpha\vec{v}) = 0, \quad (16)$$

$$\vec{v} + \vec{I}\frac{\mu_1 - \mu_2}{\mu} = -\frac{K}{\mu}(grad\,P - \rho\vec{g}), \quad (17)$$

where

$$P = sp_1 + (1-s)p_2 + (1-s)(p_{c12}|_{s=0} - p_{c12}|_{s=s}).$$

Taking into account, that for the two phases $p_2 = p_1 - p_{c12}|_{s=0}$ one obtains a different equivalent form for the equation (17) :

$$\vec{v} + \vec{I}\frac{\mu_1 - \mu_2}{\mu} = -\frac{K}{\mu}(gradp_1 - (1-s)p_{c12}(s) - \rho\vec{g}). \quad (18)$$

Analysis of equations (17, 18) shows that the term, containing the mixing flux $\vec{I}$ turns to be of low importance for fluids of close viscosities and disappears for fluids of equal viscosities. That term could also be neglected under the conditions of frontal displacement, when $\vec{u}_1 \approx \vec{u}_2 \approx \vec{v}$. In the absence of bulk pressure gradients and gravity forces the capillary forces present in the second term in the right hand side of (18) become the main driving forces determining the bulk flow velocity.

Thus the mixing flux $\vec{I}$ and capillary factor Ψ_{12} should be determined in independent experiments. The necessary experimental procedures and theoretical derivations to develop the model parameters were described in [10-11]. The values of capillary factors for fluid filtration into unsaturated porous medium were determined. In case porous medium is partially saturated by a wetting fluid the effective cross-section area of pores would be reduced that would bring to an increase of the effective capillary factor as compared to $\Psi^{w}{}_{12}$ determined in imbibition into unsaturated media:

$$\Psi_{12} = \Psi^{w}{}_{12}\frac{r_{ef}}{r_{ef} - \Delta r} = \frac{\Psi^{w}{}_{12}}{\sqrt{1-s}}. \quad (19)$$

3. Results of numerical investigations

Inhomogenity normally present in porous media, brings to a multidimensional spatial structure of the sample that could influence the capillary driven filtration. Numerical investigation of capillary driven imbibition into unsaturated inhomogeneous sample was undertaken.

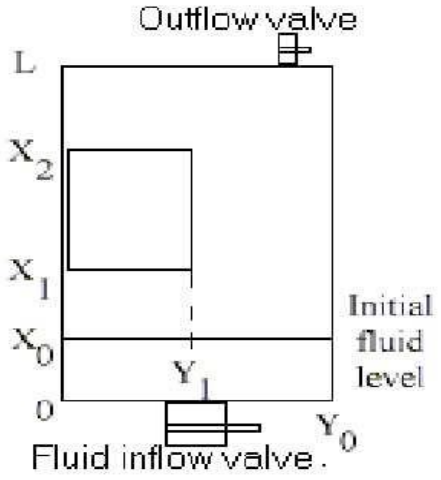

Fig. 1. The scheme of a porous medium filled cell used in physical experiments and numerical simulations. Porous medium inside the cell incorporates a zone of different permeability: $X_1<x<X_2$, $0<y<Y_1$.

The typical 2D cell with permeability inhomogenity is shown in the Fig.1. Two different scenario of imbibition were regarded: 1) $K_2<K_1$ and 2)) $K_2>K_1$. The numerical modelling was performed using the determined ψ-factor value.

The succession of images (Fig. 2) illustrates the fluid saturation maps and flow velocities for different times for both fluid phases: the displacing liquid and the displaced gas. The results were obtained for the following values of governing parameters: $K_1 = 10^{-9}m^2$, $K_2 = 10^{-10}m^2$, $\psi = 1.0$, $x_0 = 10$ mm, $x_1 = 25$ mm, $x_2 = 75$ mm, $y_0 = 100$ mm, $y_1 = 50$ mm, L = 100 mm, $\mu_1=10^{-3}$kg/(m·s), $\mu_2=10^{-3}$kg/(m·s), $\sigma_{12}=5\cdot10^{-2}$kg/s^2.

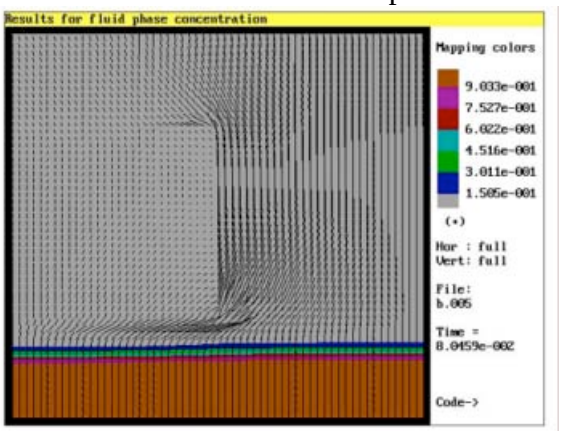

Fig. 2a.

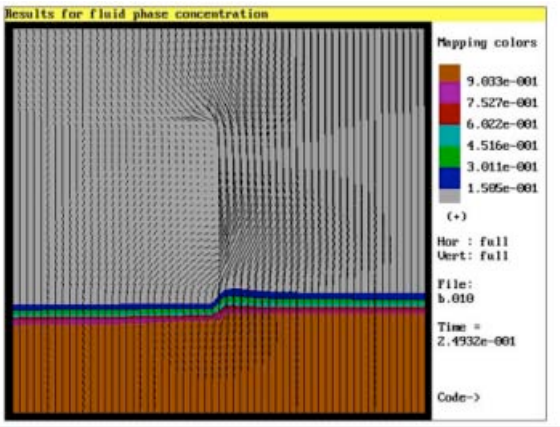

Fig. 2b.

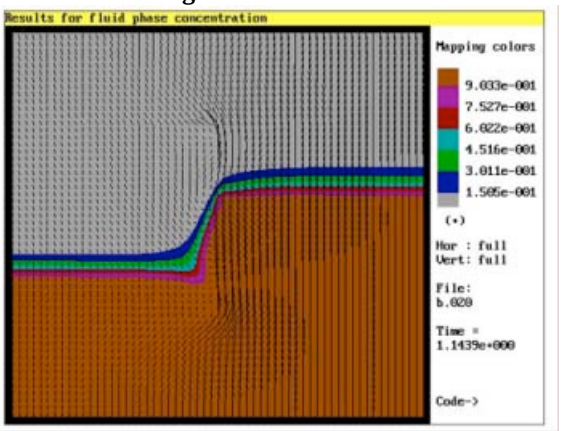

Fig. 2c.

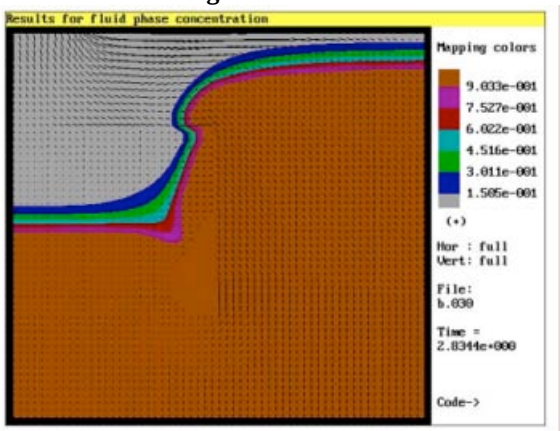

Fig. 2d.

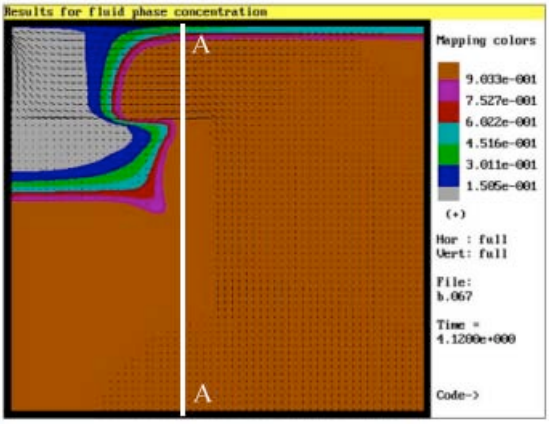

Fig. 2e.

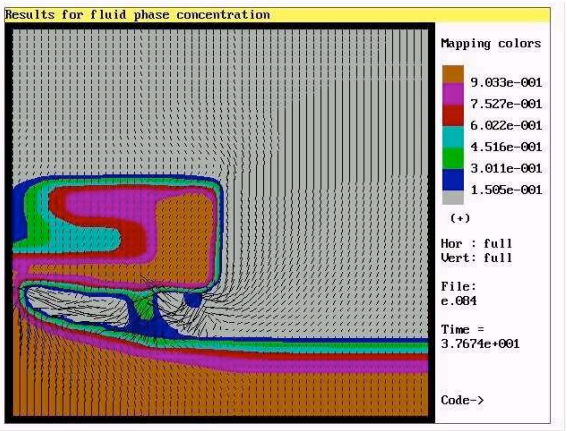

Fig. 2f.

Fig. 2. Fluid saturation maps and velocity fields obtained for successive times in numerical simulations of fluid imbibition and drainage in a porous sample incorporating a zone of lower permeability: *a-e* - imbibition, *f* - drainage.

The results show that capillary driven imbibition brings to the gas outflow from the sample. The velocity field in gas is not uniform: maximal flow rates are in the high permeable zone. On approaching the zone of lower permeability fluid velocity decreases due to the damping by the gas slug entrapped between the fluid interface and the low permeable zone. The displacement front in the low permeable zone lags behind the front in the high permeable zone, due to the increasing drag forces as well. Thus the interface curvature occurs, and finally the liquid in the high permeable zone overtakes the one in the low permeable zone thus creating a tendency to entrapping the remaining gas in the zone of low permeability. Those results are obtained for capillary driven imbibition under zero gravity conditions. The presence of gravity could change the picture not only quantitatively but qualitatively as well.

The drainage of fluid from the porous cell incorporating inhomogenity was also investigated numerically. In numerical experiments changing imbibition for drainage was achieved by applying a $2\vec{g}$ gravity acceleration at a definite moment and keeping it constant for some period of time. The present scheme of the numerical experiment simulates the conditions of low gravity experiments in aircraft parabolic flights. Under the conditions of parabolic flights the successive free-fall parabolic trajectories of the aircraft (20-25 seconds) are changed for the climbing trajectories characterised by $1.7 - 2.0\vec{g}$.

Fig.2*e* illustrates one of the stages of the drainage of fluid from the saturated inhomogeneous porous sample. The results of numerical modelling show, that drainage brings at first instant to flattening the interface and fast saturation of the low-permeable zone in the left hand side. Drainage takes place much faster in the high-permeable zone in the right hand side, while fluid saturating the low-permeable zone is entrapped there. The rapid decrease of the level of fluid in the sample brings to a formation of an air-filled gap below the low-permeable zone separating the entrapped fluid from the main flow. Due to saturation non-uniformity within the entrapped fluid a liquid bridge is being formed in a definite place below the entrapped. The further drainage of fluid from this zone takes place through the liquid bridge.

The results show that the flow pattern is strongly non-uniform and multidimensional. Thus, to register such flows in experiments one needs to apply techniques enabling to take into account their multidimensional character. For example, detecting the displacement front trajectory along the A–A line (Fig. 2) one could come to a situation under which the phase interface would be detected not sequentially along A–A, but arbitrary appearing in different places. A typical example is shown in the Fig. 3. The detected velocity would be not the actual velocity of imbibition, but the visible velocity of the phase interface intersection with the line A–A. Thus, the detected by the 1D techniques velocity could be both much smaller and much larger than the actual velocity. This possibility was taken into account in developing the software for processing the experimental results.

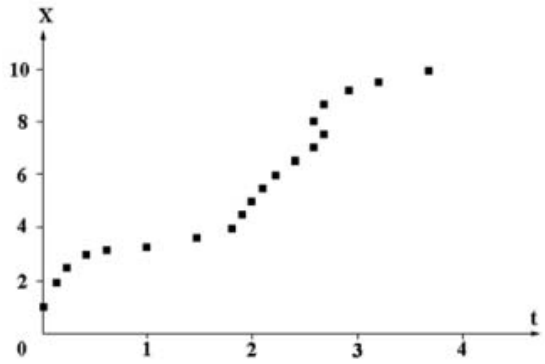

Fig. 3. Displacement front trajectory in the A-A cross-section.

4. Experimental investigations

Experiments on imbibition and drainage of a wetting fluid (water) in an artificial porous

medium composed of glass spheres were performed during aircraft parabolic flights. The gravity level varying from 0-g to 1.7-g allowed to investigate both the capillary driven imbibition of water into unsaturated sample and the drainage caused by the increase of gravity. The experimental techniques is described in details in [8]. Here we'll concentrate our attention on the peculiarities of filtration in a media containing permeability inhomogenity. The zones of different permeabilities were arranged in the experimental cells using glass balls of different diameters (Fig.4). The assembled experimental cells are shown in Fig. 5.

On reducing the gravity level the capillary driven imbibition of fluid into unsaturated initially dry porous sample begins. The phase interface remains relatively flat in a homogeneous zone (Fig. 4a). On approaching the zone of lower permeability the interface becomes curved (Fig. 4b), the capillary creeping is faster in the zone of high permeability (Fig. 4c). The phase interface in the low permeable zone lags behind the one in a high permeable zone that is in a good agreement with the results of our numerical modelling (Fig. 2a-e). On increasing the gravity level the drainage of fluid from the sample begins (Fig. 4d,e). The drainage goes faster in the zone of high permeability as well. Some part of fluid remains entrapped in the zone of low permeability (Fig. 4d). Liquid bridges are being established between the entrapped fluid and the saturated zone (Fig. 4d,e) through which evacuation of fluid from the zone of entrapment continues after the phase interface goes down far below the zone of low permeability (Fig. 4e). But some fluid still remains in the zone of low permeability.

On reducing the gravity level for the second time (entering the new parabola) capillary driven imbibition begins again in the cell (Fig. 4f,g,h). This time it goes faster as the medium was preimbibitted. On approaching the zone of low permeability the phase interface again changes its curvature, but this time the capillary driven filtration in the zone of low permeability containing the residual entrapped fluid goes much faster (Fig. 4f). The phase interface in the zone of high permeability lags behind the one in the zone of low permeability. By the time it goes up to the middle level (Fig. 4g) the whole zone of low permeability is already saturated. The reistablished liquid bridges between that zone and the main flow supply it with fluid.

The experimental results show the important role of liquid bridges established in the zones of permeability gradients and initial saturation in determining the regimes of capillary driven filtration.

To perform the quantitative comparison of experimental results with the developed theoretical model it was necessary to digitise the images with the frequency 2 images per second and reconstruct the trajectory of the phase interface to be compared with results of numerical modelling accounting for the actual gravity variation data supplied by the accelerometer.

The residual microgravity accelerations are nearly twice lower during the first parabola (g=0.05…0.06g_0) as compared with that during the second parabola (g=0.09…0.10g_0). Nevertheless, imbibition in the zone with high permeability takes place much slower during the first parabola, because the medium is initially dry and the capillary factor is lower. On approaching the zone of lower permeability the flow turns to be faster in the zone of higher permeability, that seems consistent with the results on filtration in homogeneous samples for the present low-gravity conditions [8]. Comparison of results of experimental investigations and numerical simulations shows that within the time interval 6s<t<10s mean velocities of phase interface in the control cross-sections are equal to V_1=4.5 mm/s, V_2=9.4 mm/s. The zone of lower permeability is only partially saturated by the end of the first parabola (Fig 4*c,d*).

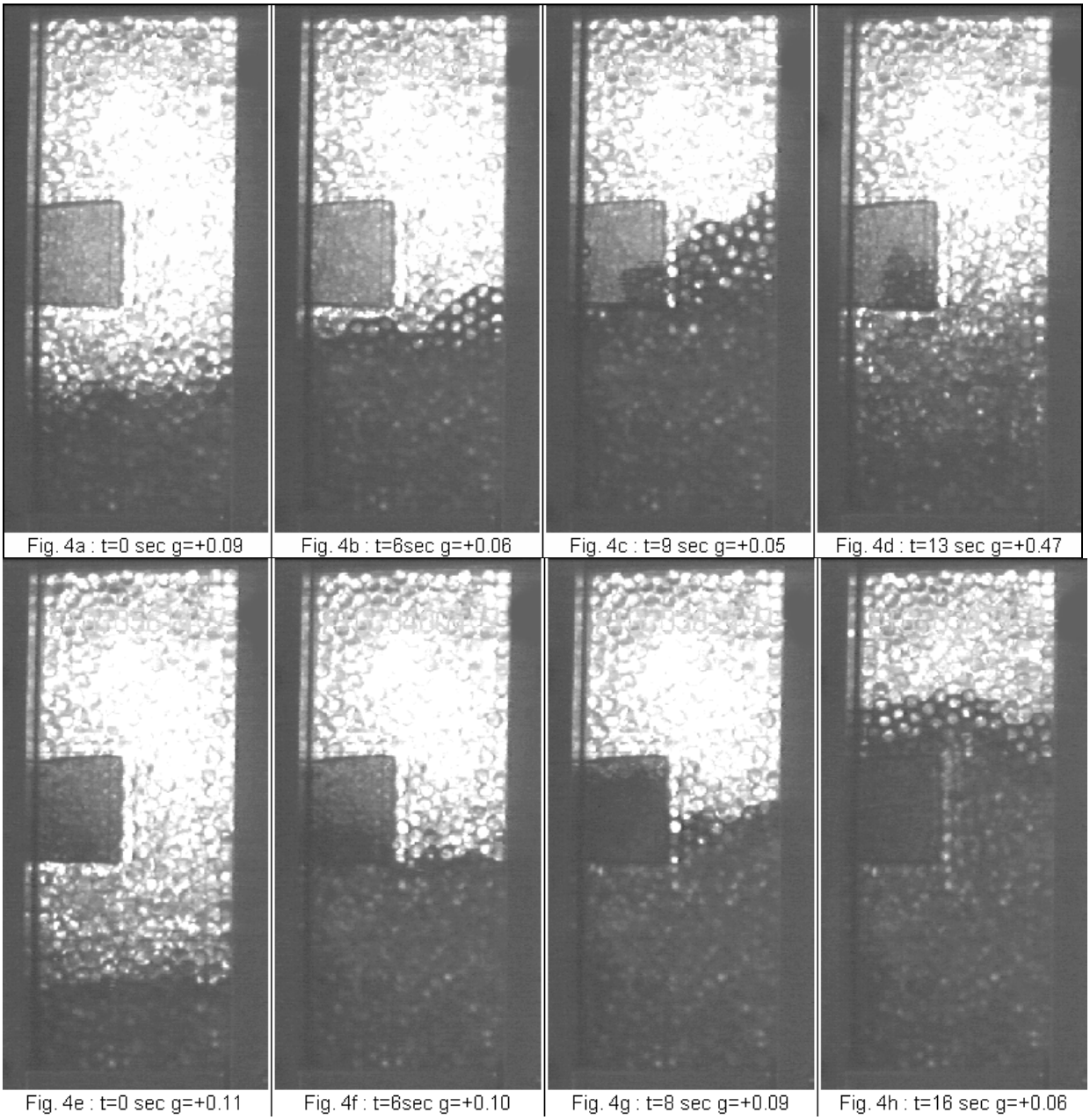

Fig. 4. Successive images for capillary driven flow of water in the cell filled in with artificial porous medium incorporating a zone of different permeability ($X_1<x<X_2$, $0<y<Y_1$) composed of glass beads of a different diameter. Experiments under variable gravity conditions: *a* - *c* - imbibition, *d* - *e* - drainage, *f* - *h* - imbibition.

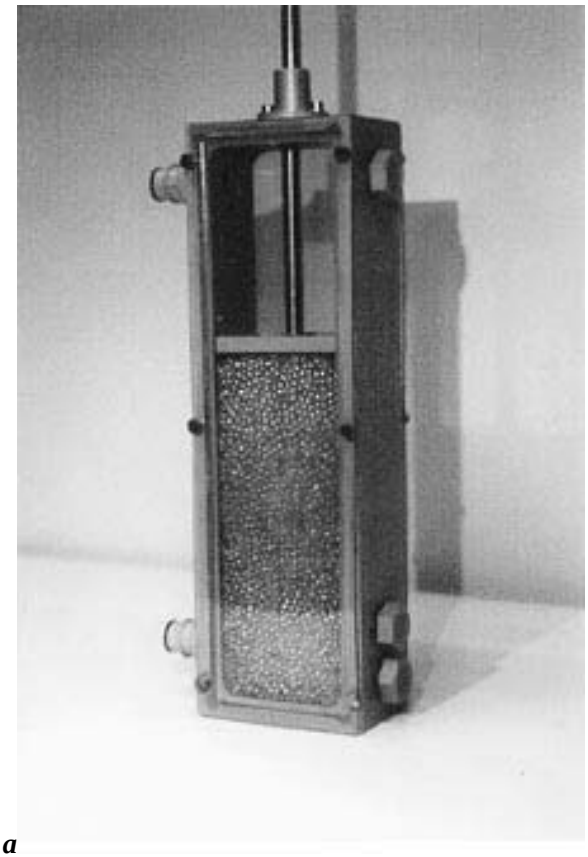

a

b

Fig. 5. Experimental cells used for capillary driven seepage flows studies under variable gravity conditions.

and turns to be a continuous zone, wherein fluid saturation changes from s_{max} in the bottom down to s_{min} on the top. The trajectories of the upper and lower boundaries of that zone are shown in Fig. 5 *b* by two solid lines appearing within the time interval $12s<t<14s$. (The boundaries were determined by analysing the grey scale level variations with the accuracy 10%.) Drainage from the zone of lower permeability takes place in a very slow manner and fluid remains entrapped in that zone for a long time. Fluid is slowly leaking from that zone through the liquid bridges, one of which is clearly seen in Fig. 4 *d*.

5. Numerical simulation of displacement instability in 3d

Theoretical and experimental studies of displacement front instability in porous media (viscous fingering) were performed, for example, in [9, 12-14]. Analytical studies of the width of fingers are present in [15]. Below we present results for 3-D unstable displacement of miscible viscous fluid from porous medium by a less viscous one are shown in Figs. 6-7. Results were obtained by numerical simulations based on mathematical models and numerical algorithms developed in [12-14].

Fig. 6 shows the influence of Péclet number. We fix the medium viscosity ratio ($M = 100$) and compare patterns of the front for different Pe ($Pe = UH / D$, U-mean flow velocity, H – channel width, D-diffusion coefficient) at aspect ratio $a = 0.5$ ($a = h / H$). The Péclet numbers increase from left to right in each row; a wide range of Péclet numbers was investigated both lower and higher than the characteristic artificial Péclet number. Each plot corresponds to some characteristic time moment. Numerical investigations showed high irregularity of the displacing zone; however, the fingers number naturally grows with the growth of the cross section area. For high a, development and splitting of the most advancing fingers looks similar; for low a, the front is bounded by the walls, and the fingers split in lower number of daughter structures. Therefore, the secondary aspect ratio is expected to influence the displacement features mostly when it is low.

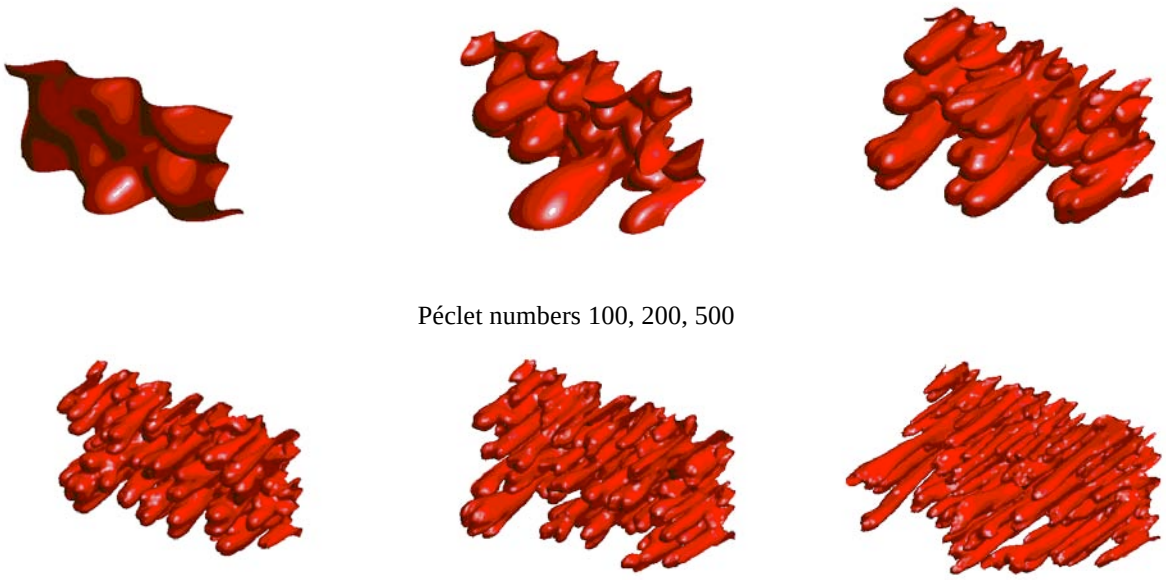

Fig. 6. *Flow patterns illustrated by displacing front surface* $s(x, y, z) = 0.25$ *for* $M = 100$, $a = 0.5$ *and various Péclet numbers.*

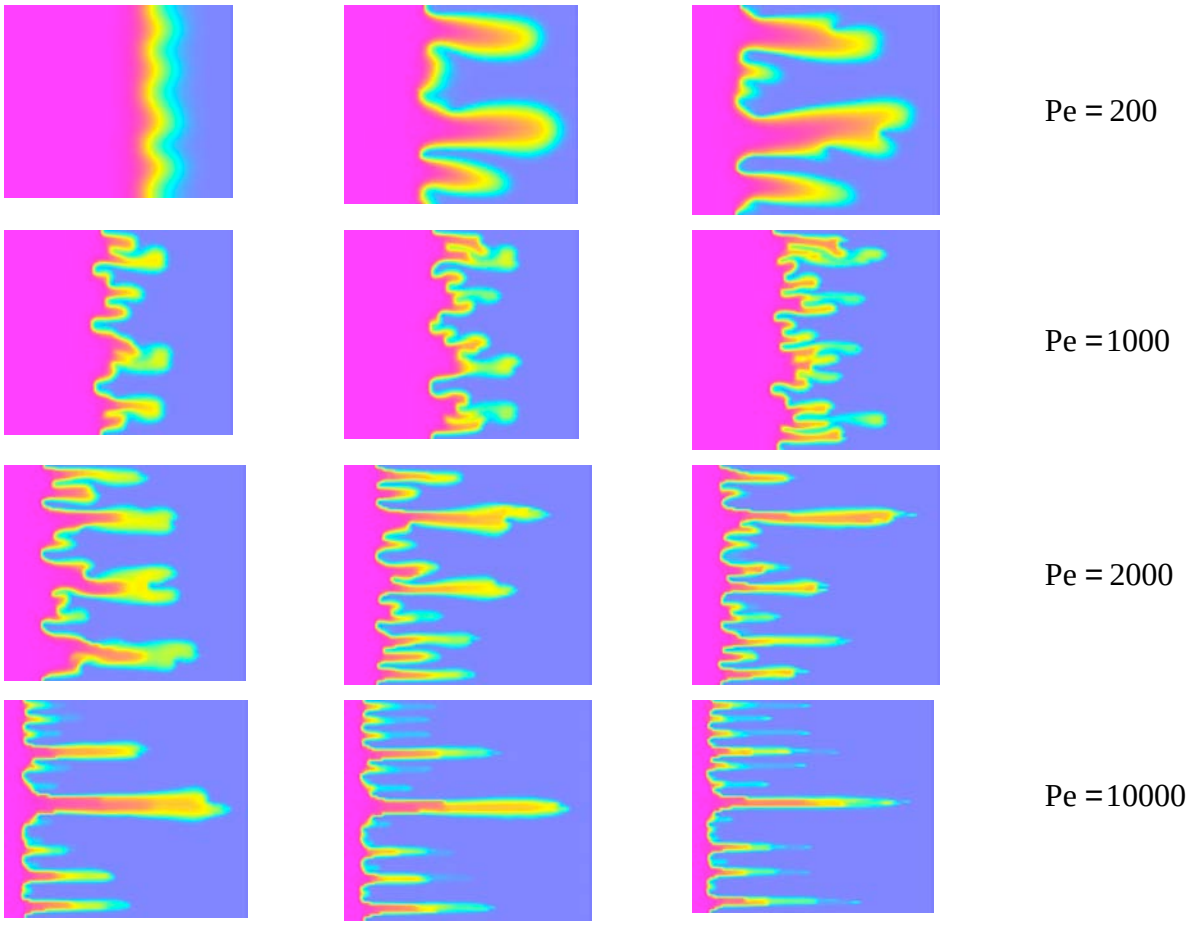

Fig. 7. *Saturation of the displacing fluid for 2D displacement process. Flow patterns for different Péclet numbers and viscosity ratios.*

Fig. 7 summarizes the flow patterns for 2D displacement simulations illustrating the saturation patterns for the displacing fluid. The flow patterns in each row are made for the same Péclet number and different viscosity ratio of displaced and displacing fluid $M = 10, 100, 1000$ (from left to right). However, two significant differences take place. First, the total number of fingers is very small compared with 3D displacement at high aspect ratio. Second, for high viscosity ratio and Péclet number, separation of tips of the fingers takes place instead of their split. We can not observe this separation on the displacement front patterns for 3D case because we monitor the surface of the displacement front there for $s = 0.25$ only, but the separated fingers have much less saturation.

Fig. 8. demonstrates the displacement front for rectangular cross-section and $a = 0.5$.

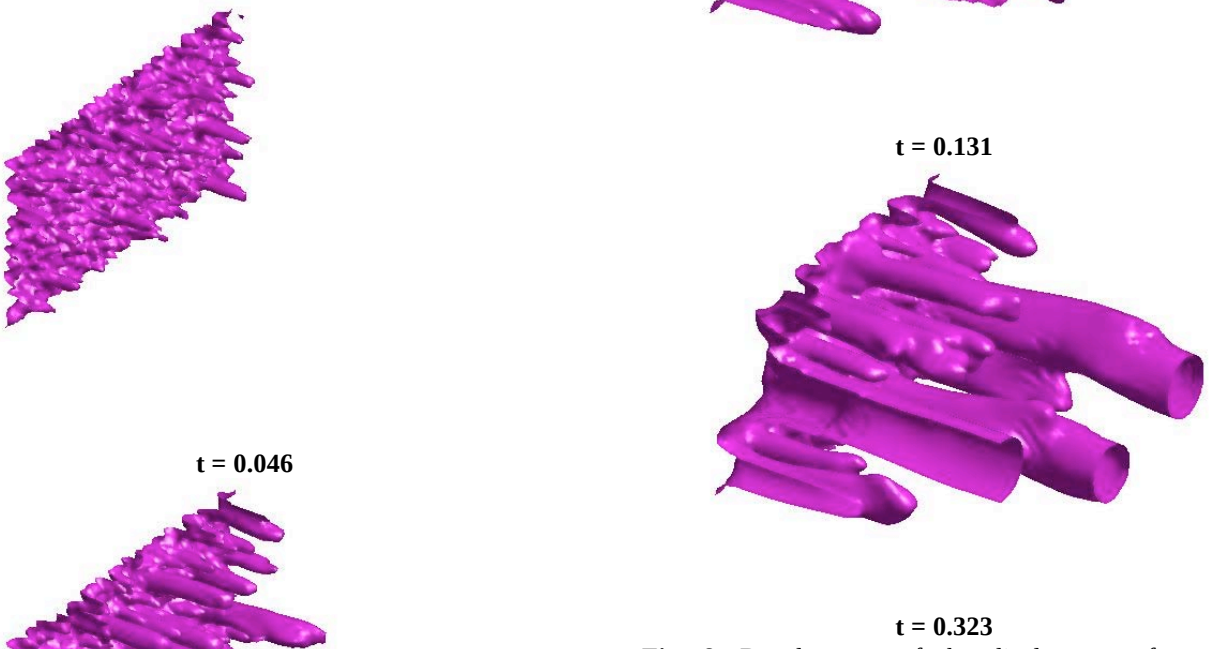

Fig. 8. Development of the displacement front for rectangular cross-section and $a = 0.5$.

It can be seen from fig. 8 that many fingers develop initially; a comparably high number of them are advancing by t = 0.069. By t = 0.098 several fingers split, three of them split into palms of daughter fingers. At t = 0.131 one of the fingers have formed a channel near a lateral wall of the domain. Two other most

advancing fingers, still split at their tips, are slowed down in their growth. At t = 0.323 they, however, reach the outflow surface, and the displacing fluid flow through the domain by three channels. One can see that qualitatively the picture is also the same except for the number of most developed fingers.

Fig. 9 demonstrates the displacement front for elliptic cross-section and $a = 0.5$.

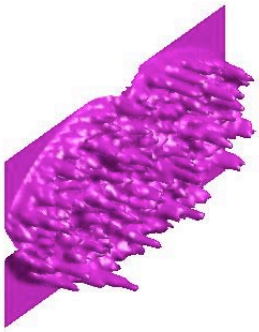

t = 0.049

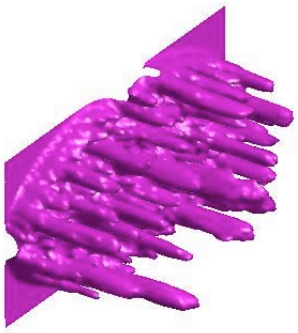

t = 0.075

t = 0.107

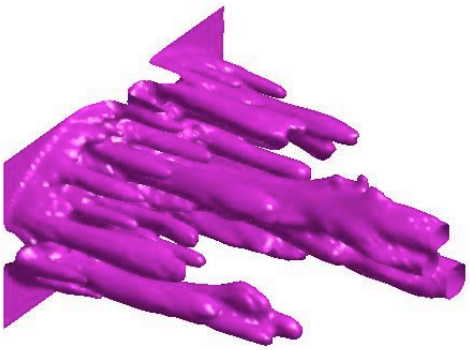

t = 0.155

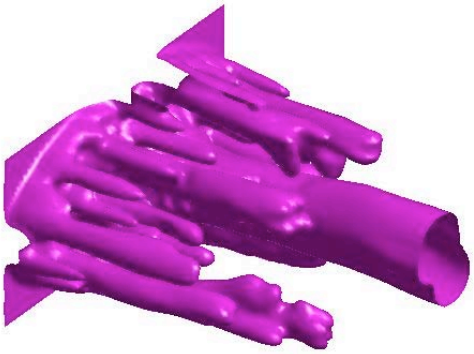

t = 0.355

Fig. 9. Development of the displacement front for elliptic cross-section and $a = 0.5$.

One can see from fig. 9, that the results for the elliptic cross section are similar to the results for the rectangular one. However, a peculiarity is seen at t = 0.155: three daughter fingers form separate breakthrough channels. With time, however, they merge into one wide channel. Only one channel is formed by t = 0.355. We expect that this difference is a result of the fundamental instability of displacement, which is very sensitive to minor perturbations, and it is not a specific peculiarity of the elliptic cross section.

5 Conclusions

Theoretical and experimental investigations of capillary driven filtration in porous media with homogeneous and inhomogeneous characteristics (permeability, porosity) carried out under microgravity conditions showed that

seepage flow regimes were very sensitive to permeability and porosity gradients in porous media.

The mathematical model for multiphase filtration in porous media under non-equilibrium conditions was developed along with experimental procedures to determine the influence of capillary forces and mixing fluxes. In contrast to the existing theories the present model does not rely on relative permeability functions for phases. Experimental and theoretical investigations showed that zones of lower permeability could serve as capillary traps for wetting fluids.

The capillary Ψ-factor determined for fluid-air interfaces in homogeneous porous samples proved to be valid for inhomogeneous samples as well thus serving a universal parameter characterising capillary properties only of a fluid pair in a porous sample.

The important role of liquid bridges established in the zones of permeability gradients and initial saturation in determining the regimes of capillary driven filtration was proved experimentally.

Instability of viscous fluid displacement by a less viscous one was simulated numerically in 2-D and 3-D cases. The role of governing parameters was studied: the thickness of viscous fingers decrease on increasing viscosity ratio and Peclet number.

Acknowledgements

The authors wish to acknowledge the support by Russian Foundation for Basic Research (Grant initiative 12-08-000198).

References

1. Barenblatt G.I., Entov V.M., and Ryzhik V.M. *Theory of Fluids Flows through Natural Rocks.* Kluwer Academic Publishers-Dordrecht / Boston / London, 1990.
2. Nigmatilin R.I. *Dynamics of Multiphase Media.* Science Publ., Moscow, 1987.
3. Kaviany M. *Principles of Heat Transfer in Porous Media.* 2nd edn. Springer-Verlag, New York, 1995.
4. Ivashnev, O.E., Smirnov, N.N. Hydraulic fracturing in a porous medium (2003) *Vestnik Moskovskogo Universiteta. Ser. 1 Matematika Mekhanika*, (6), pp. 28-37.
5. Smirnov, N.N., Tagirova, V.R. Self-similar solutions of the problem of formation of a hydraulic fracture in a porous medium (2007) *Fluid Dynamics*, 42 (1), pp. 60-70.
6. Yendler BS, Webbon B, Podolski I, Bula RJ. Capillary movement of liquid in granular beds in microgravity. *Advances in Space Research* 1996, 18 (4/5): pp. 233-237.
7. Smirnov N.N., Dushin V.R., Legros J.C., Istasse E., Boseret N., Mincke J.C., Goodman S. Multiphase Flows in Porous Medium – Mathematical Model and Microgravity Experiments. *Microgravity Science and Technology*, vol. IX(3), 1996, 222-231.
8. Smirnov N.N., Nikitin V.F., Norkin A.V., Kudryavtseva O.V., Legros J.C. , Istasse E., Shevtsova V.M., Capillary Driven Filtration in Porous Media. *Microgravity Science and Technology. Hanser Publ. 1999, vol. XII/1, pp. 23-35.*
9. Smirnov N.N., Nikitin V.F., Maximenko A., Thiercelin M., Legros J.C. Instability and mixing flux in frontal displacement of viscous fluids from porous media. *Physics of Fluids, 2005, vol.17, 084102.*
10. Smirnov, N.N., Nikitin, V.F., Legros, J.C., Istasse, E., Schramm, L., Wassmuth, F. Microgravity investigations of capillary-driven imbibition and drainage in inhomogeneous porous media (2003) *Acta Astronautica*, 54 (1), pp. 39-52.
11. Smirnov, N.N., Legros, J.C., Nikitin, V.F., Istasse, E., Schramm, L., Wassmuth, F., Hart, D.A. Filtration in artificial porous media and natural sands under microgravity conditions (2003) *Microgravity Science and Technology*, 14 (2), pp. 3-28.

12. Smirnov N.N., Nikitin V.F., Dushin V.R., Maximenko A., Thiercelin M., Legros J.C. Instability in displacement of viscous fluids from porous specimens, *Acta Astronautica, 2007, vol. 61, No 7-8, pp. 637-643.*

13. Smirnov, N.N., Nikitin, V.F., Ivashnyov, O.E., Maximenko, A., Thiercelin, M., Vedernikov, A., Scheid, B., Legros, J.C. Microgravity investigations of instability and mixing flux in frontal displacement of fluids (2004) *Microgravity Science and Technology*, 15 (2), pp. 35-51.

14. Smirnov, N.N., Nikitin, V.F., Dushin, V.R., Phylippov, Yu.G., Nerchenko, V.A. Three-dimensional convection and unstable displacement of viscous fluids from strongly encumbered space (2010) *Acta Astronautica*, 66 (5-6), pp. 844-863.

15. Logvinov, O.A., Ivashnyov, O.E., Smirnov, N.N. Evaluation of viscous fingers width in Hele-Shaw flows (2010) *Acta Astronautica*, 67 (1-2), pp. 53-59.